Correlation between experimental and theoretical approaches in the performance of new epoxy resin as an effective corrosion inhibitor for mild steel in acid pickling bath

Z. El-kiri,[1] K. Dakhsi,[1,2] N. Dkhireche,[1] A. Hmada,[1] H. Bidi,[1] F. Benhiba,[3] M. Galai,[1]* R. Hsissou,[4,5] A. Habsaoui[1] and M. Ebn Touhami[1]

[1]*Laboratory of Advanced Material, Engineering Process, Department of Chemistry, Faculty of Sciences, University Ibn Tofail, BP 242, 14000 Kenitra, Morocco*
[2]*National Center for Scientific and Technical Research (CNRST), BP 8027 N.U. Rabat 10102, Morocco*
[3]*Higher Institute of Nursing Professions and Health Techniques of Agadir Annex Guelmim, Morocco*
[4]*Laboratory of Organic Chemistry, Catalysis and Environment. Faculty of Sciences, Ibn Tofail University, BP 242, 14000 Kenitra, Morocco*
[5]*Laboratory of Organic Chemistry, Bioorganic and Environment, Chemistry Department, Faculty of Sciences, Chouaib Doukkali University, El Jadida, Morocco*
**E-mail: galaimouhsine@gmail.com*

Abstract

In this work, a new epoxy resin named 2,3,5,6-tetraglycidyloxy-4-(3,4,5-triglycidyloxy)-6-(glycidyloxymethyl)tetrahydro-2*H*-pyran-2-yloxyhexanal (OER) was synthesized and characterized using FTIR spectroscopic techniques. The corrosion inhibiting performance of mild steel in a 1 M HCl corrosive medium was evaluated through electrochemical techniques, including potentiodynamic polarization (PDP), electrochemical impedance spectroscopy (EIS), and electrochemical frequency modulation (EFM) measurements. The topological analyses of the surface were performed using scanning electron microscopy coupled with energy dispersive X-Ray spectroscopy (SEM/EDS). Theoretical calculations (DFT and MD simulation) were employed to confirm the obtained results. For the three electrochemical techniques, the inhibitory efficiencies of the OER product increased with the concentration, reaching their peak values at a concentration of 10^{-3} M (95.32% for PDP, 94.78% for EIS, and 92.31% for EFM). Additionally, the PDP method indicated that the inhibitor acted as a mixed-type inhibitor with anodic dominance in a 1 M HCl medium. The increase in temperature leads to a slight decrease in the inhibitory effectiveness of mild steel in 1 M HCl medium in the presence of 10^{-3} M of OER. This inhibitor exhibited chemical type adsorption, occurring according to the Langmuir approach. The SEM/EDS analyses specifically highlighted the corrosion inhibiting properties of the OER inhibitor. Theoretical methods provided molecular-level information by determining the natures of the active centers that contributed to the effectiveness of the OER inhibitor, as well as the nature of the bonds occurring between the OER molecules and the steel surface.

Received: December 16, 2023. Published: May 3, 2024 doi: 10.17675/2305-6894-2024-13-2-10

Keywords: *OER epoxy resin, FTIR analysis, anticorrosive protection, PDP/EIS/EFM, SEM/EDS characterization, DFT/MD simulation.*

1. Introduction

Corrosion is an undesirable universal phenomenon affecting several industrial sectors, including petroleum, chemical, and metallurgical industries. For example, taking the direct and indirect losses and preventive and protective measures into account, Jayaherdashti [1] estimated the cost of losses due to corrosion in a given country from 1% to 5% of the GNP.

Steel and its alloys are among the preferred materials in industrial engineering due to their excellent electrical, thermal and mechanical properties and their low cost [2, 3]. Despite these advantages, steel remains very sensitive to wet and aggressive environments that alter its physical-chemical characteristics. To remove rust, impurities and unwanted scales during the industrial processes, steel is subjected to treatments in pickling, cleaning and descaling baths and also during the stimulation of oil and gas wells by aggressive solutions of an acid nature such as hydrochloric acid and sulfuric acid [4]. These acids cause the dissolution of steel according to chemical or electrochemical reactions. Due to these serious effects of corrosion, different techniques have been adopted to stop or rather reduce this phenomenon. However, one of the most effective methods is to intervene in the corrosive environment by adding corrosion inhibitors [5].

Corrosion inhibitors are chemical substances added in low concentrations to corrosive media to stop or attenuate the corrosion phenomenon [6]. These inhibitors can be classified in different ways (By field of application, according to the mode of action or according to the nature of the inhibitor molecule). Mineral inhibitors are generally very effective, but often cause ecological problems such that the majority of them are non-biodegradable, dangerous and harmful to the environment [7, 8]. On this basis, and in order to counteract the phenomenon of corrosion, numerous researchers have resorted to the adoption of organic inhibitors such as polymers and poly epoxides (epoxy polymers). Organic inhibitors are often environmentally friendly, on the other hand their chemical structure is rich in heteroatoms (O, N, S), functional groups (−NH, −N=N−, −C=N−, −CHO, R−OH) and in multiple bonds (double and triple). As a result, these organic molecules are adsorbed on the steel surface through physical and/or chemical bonds, thus forming a protective film that reduces the corrosion rate [9]. Inhibitors based on polymers and epoxides soluble in acid solutions have an excellent effectiveness, even at low concentrations [10]. This characteristic is due to the fact that these inhibitors are composed of giant organic molecules that allow them on the one hand to cover a large metal surface and on the other hand to contain a huge number of heteroatoms of unsaturated bonds, aromatic rings and functional groups. For this reason, some researchers have preferred to adopt this type of inhibitor to fight against the corrosion phenomenon. Among these inhibitors, diglycidyl amino benzene (DGAB) is worth mentioning [11], N^2,N^4,N^6-tris(2-(oxiran-2-ylmethoxy)ethyl)-N^2,N^4,N^6-tris(oxiran-2-ylmethyl)-2,4,6-triamine-1,3,5-triazine (ERT) [12], ethylene tribisphenol A triglycidyl ether (TGETBAE) [13], decaglycidyl pentamethylene dianiline of phosphorus (DGPMDAP) [14].

In this paper, and after synthesis of a new poly epoxy (2,3,5,6-tetraglycidyloxy-4-(3,4,5-triglycidyloxy)-6-(glycidyloxymethyl)tetrahydro-2*H*-pyran-2-yloxyhexanal (OER), a study of its effect on the corrosion inhibition of steel in acidic environment will be made. For this purpose, and to characterize the inhibitor (OER) and evaluate its performance, spectroscopic (FTIR), electrochemical (steady, transient, EFM) and surface topology (SEM, AFM) techniques will be performed. Finally, and to confirm the results, theoretical calculations and molecular dynamics simulations will be employed.

2. Materials and Methods

2.1. Synthesis of octafunctional epoxy resin (OER)

All used chemical products employed in this work namely maltose (monohydrate) (99%), epichlorohydrin (99%), methanol (99%) and triethylamine (99.5%) were purchased from Sigma Aldrich. All chemical products were used without other purification. A novel octafunctional epoxy resin, namely 2,3,5,6-tetraglycidyloxy-4-(3,4,5-triglycidyloxy)-6-(glycidyloxymethyl)tetrahydro-2*H*-pyran-2-yloxyhexanal (OER), was synthesized and developed by using a condensation reaction in two steps according to the experiment procedure indicated by Hsissou *et al*. [15, 16]. In the first step, in a balloon of 100 mL fitted with refrigerant, 2.77×10^{-3} mol of maltose was condensed with 2.23×10^{-2} mol of epichlorohydrin in the presence of methanol as a solvent under magnetic stirring at 70°C for 8 h (Scheme 1). In the second step, 4.57×10^{-2} mol of triethylamine as basis was added to reaction mixture to obtain the octafunctional epoxy resin under magnetic stirring at 40°C for 4 h (Scheme 1). Additionally, methanol and triethylamine excess were removed by using the rotary evaporator. Finally, a white resin with a good yield (92%) was obtained.

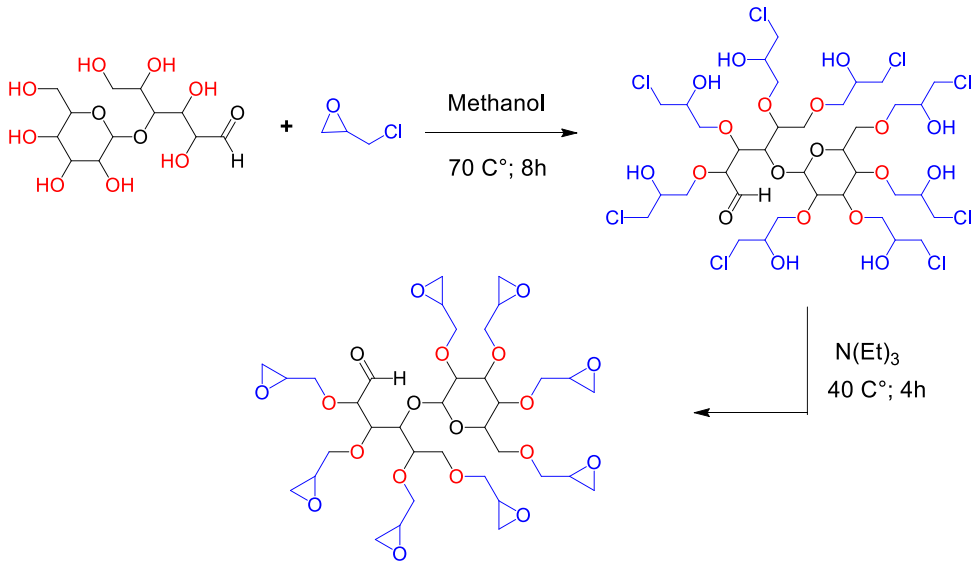

Scheme 1. Synthesis of octafunctional epoxy resin (OER).

2.2. Materials, electrolyte and techniques used

The examined samples were obtained by cutting mild steel metal plates, and the chemical composition of this steel is listed in Table 1. The samples were cut into rectangular pieces with dimensions of 2.5×1.0×0.05 cm.

Table 1. Composition of the steel samples studied.

Elements	C	Co	Si	Mn	Ti	Cr	Ni	Cu	Mo	V	Al	W	Fe
% by weight	0.11	0.0012	0.36	0.47	0.24	0.12	0.1	0.14	0.02	0.03	0.03	0.06	The rest

Before each use, each sample intended for use as a working electrode undergoes a pre-treatment process. This process begins with mechanical polishing of the electrode surface using progressively finer abrasive papers (500, 1200, 1500, 2000). Subsequently, the electrode is thoroughly rinsed with distilled water, then cleaned with acetone and bidistilled water. Once cleaning is complete, the electrode is left to air dry. Finally, it is quickly immersed in the electrochemical cell containing the aggressive solution.

The 1 M HCl solution is obtained by diluting concentrated acid from the Riedel de Haen brand, characterized by a density of 1.19 and a purity of 37% by weight.

Stationary and transient electrochemical measurements were performed using a potentiostat/galvanostat PGZ100 controlled by Volta Master 4 analysis software. The electrochemical experiments were conducted in a three-electrode cell, using a steel plate as the working electrode (exposed surface of 1 cm^2), a platinum rod as the counter electrode, and an Ag/AgCl electrode as the reference electrode. Electrochemical impedance spectroscopy (EIS) measurements were carried out at the open circuit potential (OCP) over a frequency range from 100 kHz to 100 mHz with 10 points per decade. The applied signal amplitude (AC) was 10 mV. All experiments were performed after immersing the steel in a 1.0 M HCl solution for 30 minutes, both in the absence and presence of various concentrations of the OER inhibitor. Potentiodynamic polarization curves were obtained by scanning the working electrode potential from –900 mV to –100 mV at a scan rate of 1 mV/s. Electrochemical frequency modulation (EFM) measurements were conducted using the Gamry Interface 1010 Potentiostat/Galvanostat/Zra analyzer, with the DC105 Corrosion software. During these measurements, a potential perturbation signal with an amplitude of 20 mV, including two sinusoidal waves at 2 Hz and 5 Hz, was applied.

2.3. DFT and MDS details

The mechanism in which OER acts on the metal surface was explored using the DFT in the aqueous phase [17]. This theoretical contribution also provided a link between the chemical reactivity indices and the estimated experimental inhibitory effectiveness of the neutral form [18]. An optimization of the OER neutral was done to the ultimate geometry at the DFT/B3LYP/6-311G++(d, p) *via* the Gaussian 09 software [19]. E_{LUMO}, E_{HOMO}, ΔE_g, χ,

global hardness "η", and the transfer of electrons from occupied organic molecule orbitals to vacant metal surface orbitals "ΔN_{110}" [20].

$$\Delta E_{\text{gap}} = E_{\text{LUMO}} - E_{\text{HOMO}} \tag{1}$$

$$\chi = \frac{1}{2}\left(E_{\text{HOMO}} + E_{\text{LUMO}}\right) \tag{2}$$

$$\eta = \frac{1}{2}\left(E_{\text{HOMO}} - E_{\text{LUMO}}\right) \tag{3}$$

$$\Delta N_{110} = \frac{\chi_{\text{Fe}_{110}} - \chi_{\text{inh}}}{2\left(\eta_{\text{Fe}_{110}} + \eta_{\text{inh}}\right)} = \frac{\Phi - \chi_{\text{inh}}}{2\eta_{\text{inh}}} \tag{4}$$

Molecular dynamics simulations (MDS) are employed to explore how OER interact with Fe(110) systems. This simulation was carried out using the Forcite module in the Materials Studio software. A simulation box (27.30×27.30×37.13 Å^3) with a 6-couche slab model for every layer creating an (11×11) unit cell was effectively applied. The volume of the vacuum 33 Å^3 occupies the part of the simulation box and is filled by the species 500 H_2O, 5H_3O^+, 5Cl^-, and OER. The Andersen thermostat in the NVT ensemble (constant number of particles *N*, volume *V*, and temperature *T*), the 1000 ps (simulation time) and 1.0 fs (time step) under the COMPASS force field, and regulated the temperature of the simulated system of 298 K [21].

3. Results and Discussion

3.1. FTIR characterization

The novel octafunctional epoxy resin, 2,3,5,6-tetraglycidyloxy-4-(3,4,5-triglycidyloxy)-6-(glycidyloxymethyl)tetrahydro-2*H*-pyran-2-yloxyhexanal (OER), was synthesized and characterized using Fourier transform infrared (FTIR) spectroscopy (BRUKER type) to identify its various functional groups. The FTIR spectrum analysis of OER octafunctional epoxy resin is displayed in Figure 1.

The absorption band appeared at 3260.32 cm^{-1} which is attributed to the stretching vibrations of hydroxyl function (–OH) of unclosed oxirane group. Further, the absorption band situated at 2945 cm^{-1} corresponding to aliphatic methylene (CH_2). Then, the absorption band located at 1738.54 cm^{-1} which is attributed to C=O of aldehyde function. In addition, the absorption bands at the 1455.22 cm^{-1}, 1434.0 cm^{-1} and 1228.76 cm^{-1} corresponding to the stretching vibrations of aliphatic C–H. Also, the absorption band appeared at 1036.0 cm^{-1} can be assigned to the asymmetric stretching vibration of C–O–C aliphatic ether function. Also, the presence of the epoxide group is shown by the characteristic absorption bands at 901.37 cm^{-1}, 868.71 cm^{-1} and 796.49 cm^{-1} which are attributed to stretching of C–O–C and C–O of oxirane group.

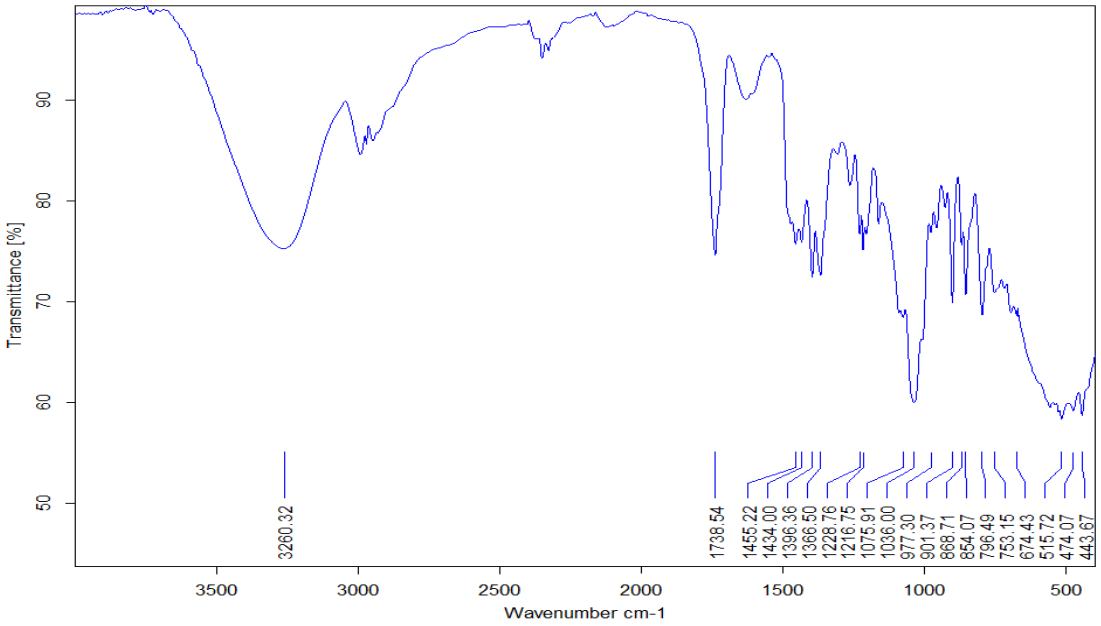

Figure 1. IR spectra of OER synthesized.

3.2. Electrochemical studies

3.2.1. Potentiodynamic study

The technique of potentiodynamic polarization (PDP) was adopted to study and assess the performance of the inhibitor concentration effect (OER) on the opposition to corrosion of steel in acid medium, HCl 1 M and at 298 K.

Figure 2 presents the polarization curves relating to mild steel in 1 M HCL medium, without and in the presence of various concentrations of inhibitor (OER), at 298 K. The electrochemical parameters are reported in Table 2.

By carefully monitoring the polarization curves, one can observe that the cathodic corrosion current densities dropped for the inhibited solutions compared to the pristine solution, accompanied by a slight variation in the cathodic slopes β_c. This reveals that the effect of the OER inhibitor has a direct impact on the reduction reaction of H^+ protons by blocking the cathodic active sites. On the other hand, the cathodic branches of the inhibited solutions remain parallel and exponential in shape, which advises that the mechanisms of cathodic reactions remain unchanged and controlled by a pure activation mechanism [22]. Similarly, for anodic plots, a significant decrease in the densities of anodic corrosion currents is observed with the addition of OER inhibitor molecules. This suggests that the OER inhibitor acted by blocking the anodic sites due to the formation of an adsorbed layer on the surface of the metal which limits its dissolution [23]. Beyond the desorption potential, the reduction in the anodic corrosion rate for the inhibited solutions was not as significant, but this rate remained lower than that of the blank. This can be attributed to a huge dissolution of the steel due to a desorption of the protective layer formed, because the desorption rate of the inhibitor exceeded its adsorption rate [22].

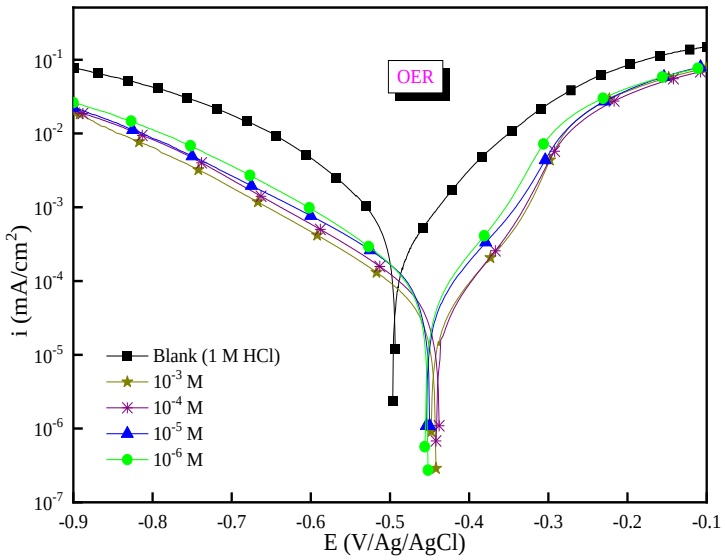

Figure 2. Polarization curves of the studied steel in 1 M HCl solutions, blank and in the presence of different concentrations of OER inhibitor at 298 K.

Table 2. Electrochemical parameters of the steel studied in 1 M HCl solutions, blank and in the presence of different concentrations of OER inhibitor at 298 K.

Medium	Conc., M	E_{corr}, mV/Ag/AgCl	i_{corr}, μA·cm^{-2}	$-\beta_c$, mV·dec^{-1}	β_a, mV·dec^{-1}	η_{PP}, %
1 M HCl	–	−498	983	140	150	–
OER	10^{-3}	−442	46	166	88	95.3
	10^{-4}	−437	56	165	93	94.3
	10^{-5}	−449	91	173	102	90.7
	10^{-6}	−452	108	170	106	89.0

Inspecting the values presented in Table 2, there is a decrease in the corrosion current and an increase in efficiency with the increase in the concentration of the OER inhibitor. This leads to the current density reaching its minimum value (46 μA·cm^{-2}), and the efficiency of the inhibitor reaching its maximum value (95.3%) at the highest concentration (10^{-3} M) of the OER inhibitor.

This is due to the formation of a barrier layer at the metal/solution interface resulting from the adsorption of the OER molecules onto the steel surface, reducing the number of active sites and consequently protecting the metal. In addition to the above, the reasons for the adsorption and excellent efficiency can be attributed to the fact that the OER molecules contain many oxygen atoms and epoxy groups, which facilitate the absorption of this inhibitor by forming an OER–Fe complex that covers the metal surface [24]. The corrosion potential underwent a shift towards the noblest potentials, with a maximum variation of

61 mv/Ag/AgCl, which has not outdated 85 mv/Ag/AgCl, which indicates that the OER inhibitor is of the mixed type, with anodic primacy [25, 26].

In spite of its necessity for the study of the phenomena of corrosion and inhibition, the PDP technique is still insufficient, mainly for the characterization of complex processes with several steps. As a result of this deficiency, the electrochemical impedance method was used.

3.2.2. Electrochemical impedance studies

The importance of the EIS technique is reflected in the fact that it allows one to perform deeper studies on different mechanisms related to corrosion inhibition, so that the fastest processes emerge at high frequency and the slowest at low frequency [27]. This method also makes it possible to know the resistive and capacitive behaviour of the interface and the distinction of reaction phenomena by their relaxation time.

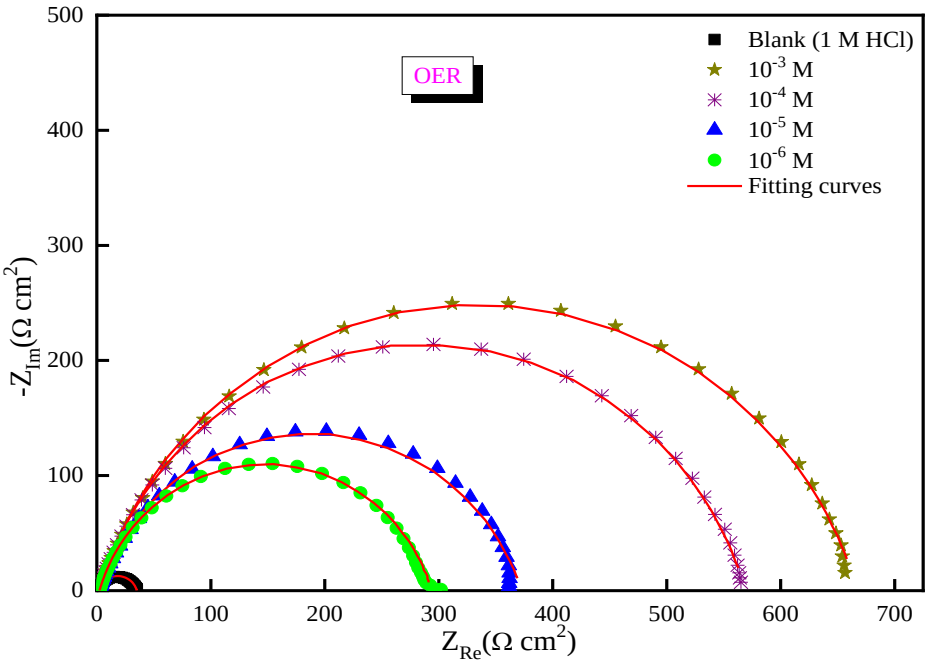

Figure 3. Impedance spectra in the Nyquist plane for steel in 1 M HCl medium in the absence and presence of various concentrations of inhibitor at 298 K.

According to Figure 3, it is clear that the Nyquist plots for the steel samples immersed in inhibited and uninhibited 1 M HCl solutions are just singular capacitive loops in the form of flattened semi-circles. The flatness of the semicircles is caused by the specificity of the electrode, which exhibits the impedance frequency dispersion caused by the roughness and inhomogeneity of the electrode surface [28]. This dispersion can be explained by the presence of impurities and dislocations, or by the adsorption of inhibitory molecules [29]. Similarly, Figure 4 indicates the presence of a single time constant following the emergence of the single peaks on the Bode plots. This validates the uniqueness of the capacitive loops mentioned above and demonstrates the control of the electrochemical mechanism by the charge transfer kinetics pure on a heterogeneous and non-regular surface [30, 31].

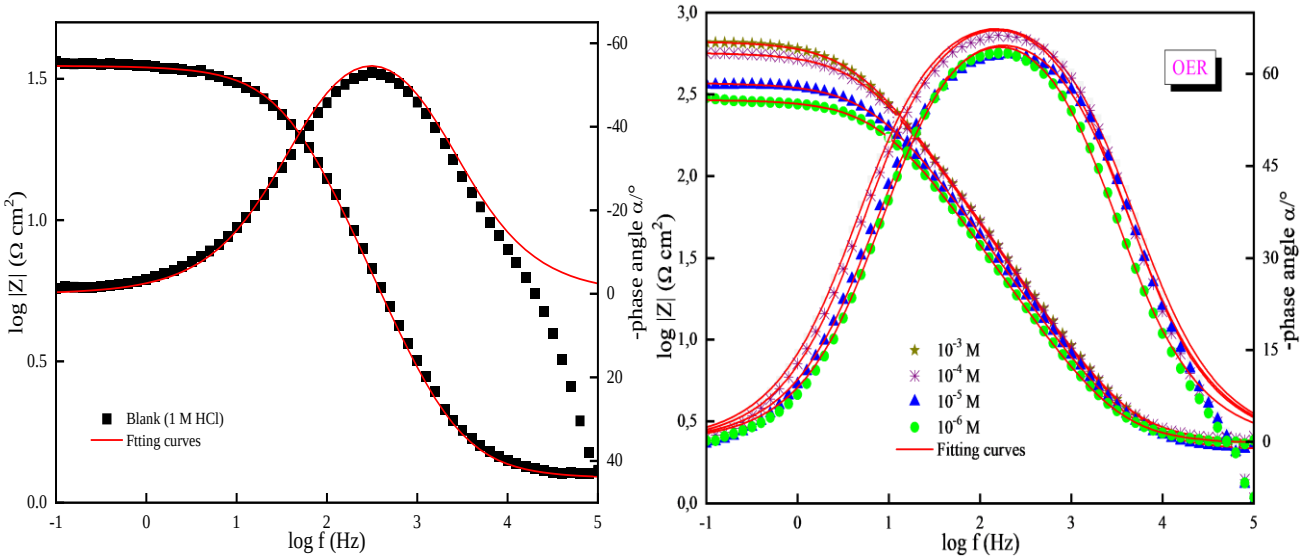

Figure 4. Bode diagrams for steel in 1 M HCl in the absence and in the presence of different concentrations of inhibitor at 298 K.

In addition to all that have been mentioned, the sizes of the loops increase with increasing concentration of the OER product, so that these arcs remain much wider than that obtained in the virgin solution. Another point to note is that the maximum phase angles in the Bode diagram increase with the content of the inhibitor in the corrosive solution. Under pretext of these results, the adsorption of OER molecules was clearly manifested, leading to a film covering the surface of the steel. Therefore, that maximum concentration performs as a wonderful protection of the metal against corrosion [32].

Following an adjustment of the capacitive loops, the impedance spectra are compared to an electrical impedance, each of the electrochemical processes of which is associated with a suitable electrical component (resistance, capacitance). The circuit in Figure 5 is composed of a solution resistor R_s in series with a shunt circuit, consisting of a charge transfer resistor R_{ct} and a constant phase element CPE (Ø). This circuit is the result of a modelling of the electrochemical mechanisms that occur at the steel/inhibited solution interface [33]. The constant-phase element appearing in the equivalent circuit comes to replace the pure capacitor, in order to achieve an adaptation of the non-ideal capacitive response at the level of the double layer [34].

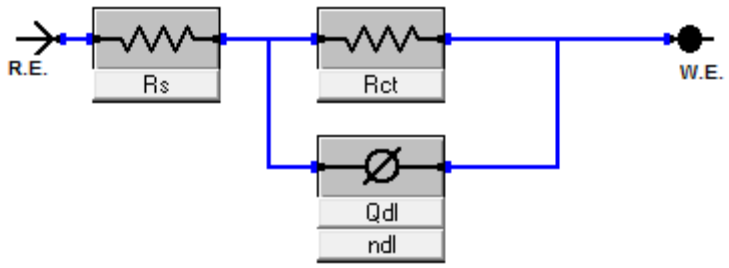

Figure 5. Equivalent electric circuit of the steel/solution interface.

The impedance of the CPE element is given by expression (5) [35]:

$$Z_{\mathrm{CPE}} = Q^{-1}(i\omega)^{-n} \tag{5}$$

where Q, i, ω and n are respectively the proportionality coefficient of the CPE, the pure imaginary number, the pulsation in rads^{-1} and the deviation parameter related to the phase shift ($-1 \leq n \leq +1$).

Expression (6) gives the value of the double layer capacitance [35].

$$C_{\mathrm{dl}} = \left(QR_{\mathrm{ct}}^{n-1}\right)^{\frac{1}{n}} \tag{6}$$

where, R_{ct} and n are successively the proportionality coefficient of the CPE, the charge transfer resistance in the presence of inhibitor and the deviation parameter linked to the phase shift.

The corrosion inhibitory efficiency (η_{imp}%) and the recovery rate θ are determined according to expressions (7) and (8):

$$\eta_{\mathrm{imp}}\% = \frac{R_{\mathrm{ct}} - R_{\mathrm{ct}}^{0}}{R_{\mathrm{ct}}} \times 100 \tag{7}$$

$$\theta = \frac{R_{\mathrm{ct}} - R_{\mathrm{ct}}^{0}}{R_{\mathrm{ct}}} \tag{8}$$

where R_{ct} and R_{ct}^{0} are the charge transfer resistances in the absence and presence of the inhibitor.

The values of efficiency, recovery rate and electrochemical parameters for different concentrations of OER are given in Table 3.

Table 3. Electrochemical parameters of the impedance diagram of the steel studied in 1 M HCl, both in the absence and presence of OER at different concentrations at 298 K.

Medium	**Conc., M**	R_s, ($\Omega \cdot cm^2$)	R_{ct}, ($\Omega \cdot cm^2$)	C_{dl}, ($\mu F \cdot cm^{-2}$)	Q, ($\mu F \cdot s^{n-1} \cdot cm^{-2}$)	n_{dl}	θ	η_{imp}, %
1 M HCl	–	1.12	34.7	121	419	0.773	–	–
OER	10^{-3}	2.189	665.5	52	97	0.816	0.948	94.8
	10^{-4}	2.369	566.6	53	95	0.833	0.939	93.9
	10^{-5}	2.114	370.2	59	122	0.807	0.906	90.6
	10^{-6}	2.319	291.3	64	130	0.821	0.881	88.1

By examining the values indicated in Table 3, it becomes apparent that there is a significant increase in the resistance of transfer of load R_{ct}, accompanied by a notable reduction in the level of the values of the capacity C_{dl} of the double layer and of the Q coefficient when the OER molecules are integrated into the aggressive solution. Similarly,

an increase in the concentration of the inhibitor leads to an increase in the of charge transfer resistance, which reaches its maximum value at the concentration of 10^{-3} M. These results can be attributed to the adsorption of inhibitor molecules on the metal surface, thus forming a barrier film capable of protecting the steel from corrosion [36]. Helmut's expression, shown in Equation 9, supports the finding of a correlation between the variation of the capacity of the double layer and the properties of the latter. This is manifested by the fact that the lowering of the capacitance C_{dl} is due to a decrease in the dielectric constant or an increase in the thickness of the double layer, thanks to the accumulation of the OER molecules on the metal surface. On the other hand, let's not forget that the value of the coefficient of inhomogeneity (n) is lower than unity, attesting to the heterogeneity of the adsorption.

$$C_{dl} = \frac{\varepsilon_0 \varepsilon}{e} S \tag{9}$$

where, e, S, ε_0 and ε are respectively the width of the double layer, the area of the working electrode, the permittivity and the dielectric constant of the medium.

Table 3 indicates that the change in efficacy is compatible with the increase in the concentration of the inhibitor. So that it reaches its maximum value of 94.8% at the highest concentration of OER molecules of 10^{-3} M. This is due, on the one hand, to the fact that the giant OER particles are likely to cover a large steel surface and thus protect it from corrosion. On the other hand, the structure of these molecules, containing a double bond, in addition to its richness in heteroatoms (oxygen atoms), which include free electrons allowing the exchange and the donor-acceptor interaction with vacant orbitals (d) iron [37].

3.2.3. Electrochemical frequency modulation (EFM)

The importance of the EIS technique is reflected in its ability to provide valuable information, such as bias resistance and metal-solution interface capacitance. Despite these advantages, this technique presents certain difficulties concerning the inaccuracy of the measurements during the low frequency disturbance [38] and the inability to make a direct measurement of the corrosion current density [39]. To address these deficits, the technique of electrochemical frequency modulation (EFM) was adopted. This technique is based on the reality that current density responses are measured through non-destructive perturbation. In other words, to carry out these measurements, two sinusoidal voltages of different frequencies are simultaneously applied to the sample, the amplitudes of which fluctuate around the corrosion potential by values of ± 10 mV to ± 20 mV. The applied voltage frequencies, which are known as harmonic or intermodulation frequencies, must be high. The measurement of corrosion current density is done through a combination of the calculation operations of addition, subtraction and multiplication of the frequencies of the applied signals, under the pretext of minimizing the background noise interference [40]. In addition to its fast performance and harmlessness to the sample, the EFM technique is also able to monitor the quality of the measurements by calculating the causality coefficients (CF-2 and CF-3) [38].

The intermodulation spectra concerning the steel placed in the 1 M HCl solution without and in the presence of OER inhibitors at various concentrations and at 298 K are given in Figure 6.

Figure 6 clearly shows that the intermodulation peaks for different inhibited and blank solutions are clearly visible and much more intense than background noise. These peaks are used to determine the various electrochemical parameters [38, 39]. These parameters, such as Tafel slopes, corrosion current densities and causal factors, are shown in Table 4.

The results presented in Table 4 clearly show the reduction of the corrosion current with the addition of the OER inhibitor in the corrosive solution. This decrease becomes more significant with the increase in the concentration of the inhibitor, which justified the excellent efficiency (92.31% at the concentration of 10^{-3} M) of the OER product in fighting against the corrosion of the steel by forming an adsorbed film on its surface. These results validate thanks to the values of the causality coefficients CF-2 and CF-3, which are close to their theoretical counterparts (2.00 and 3.00 respectively).

The results determined by the three techniques PDP, EIS, and EFM are consistent, which validates the study.

Table 4. Corrosion parameters obtained by EFM for corrosion of steel in 1 M HCl solution in the absence and presence of OER.

Medium	Conc. M	i_{corr}, μA·cm^{-2}	β_a, mV·dec^{-1}	$-\beta_c$, mV·dec^{-1}	*CR*, mm·yr^{-1}	CF-2	CF-3	%η
1 M HCl	Blank	755	162	177	344.9	1.52	2.86	–
OER	10^{-3}	58	172	131	26.91	1.97	3.22	92.3
	10^{-4}	62	162	115	28.58	1.93	3.05	91.8
	10^{-5}	80	152	117	36.74	1.84	2.90	89.4
	10^{-6}	85	153	108	38.78	1.84	2.79	88.7

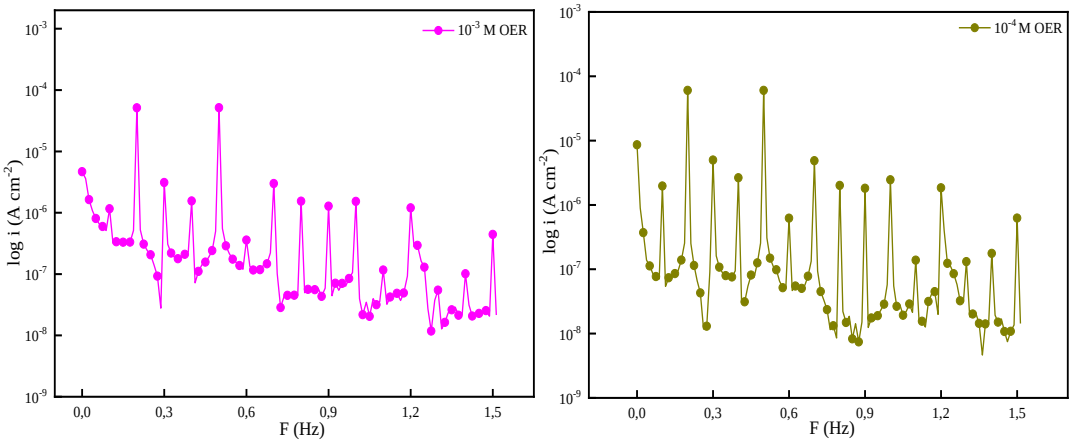

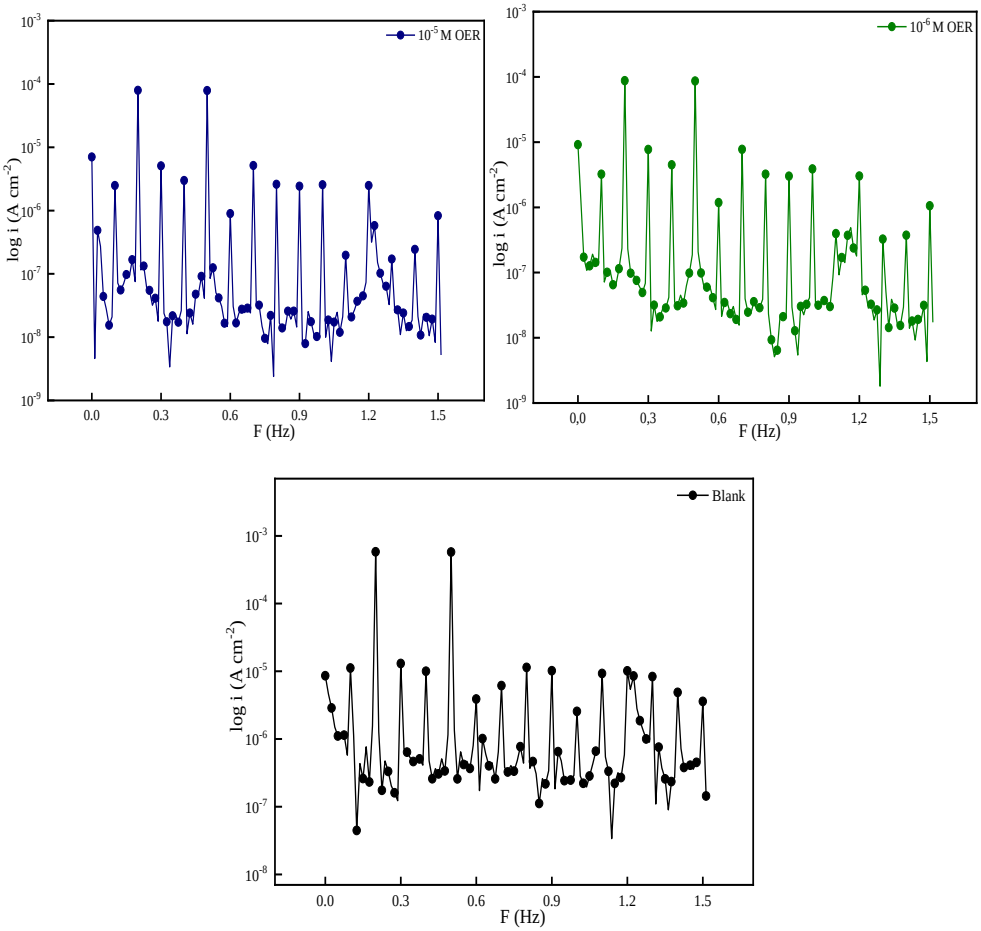

Figure 6. Intermodulation spectra for steel in 1 M HCl solution without and in the presence of OER inhibitors at various concentrations and at 298 K.

3.3. Adsorption isotherm

In order to fully understand the electrochemical mechanisms of the interactions leading to the adsorption of inhibitory molecules on the metal surface, the use of adsorption isotherms remains a mandatory necessity [37]. Among these most commonly used isotherms are Langmuir, Temkin and Frumkin, whose expressions are given by the following equations [41]:

Langmuir isotherm:
$$\frac{C_{\text{inh}}}{\theta} = \frac{1}{K_{\text{ads}}} + C_{\text{inh}} \tag{10}$$

Temkin isotherm:
$$\exp(-2\alpha\theta) = K_{\text{ads}} C_{\text{inh}} \tag{11}$$

Frumkin isotherm:
$$\frac{\theta}{1-\theta}\exp(2\alpha\theta) = K_{\text{ads}} C_{\text{inh}} \tag{12}$$

where θ, α, K_{ads} and C_{inh} are respectively the surface coverage, the molecular interaction constant, the adsorption equilibrium constant and the concentration of the inhibitor in the electrolyte.

After experimenting with these models, Langmuir's approach was found to be the most appropriate for the study.

The Figure 7 illustrates the variation of the quotient, of the concentration of inhibitor and of the recovery rate, C_{inh}/θ as a function of the variation in concentration C_{inh}.

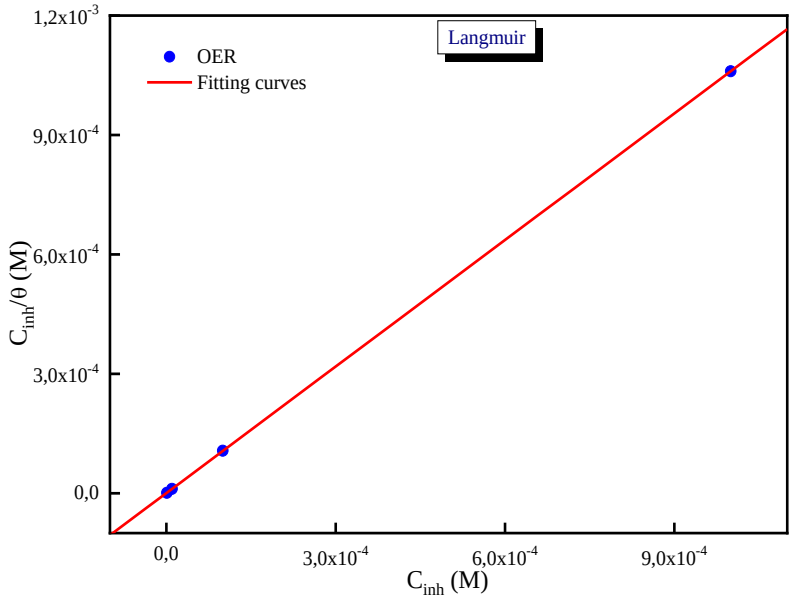

Figure 7. Langmuir isotherm for mild steel in 1 M HCl solution at 298 K in existence of the OER inhibitor.

By exploiting the plot of the Langmuir isotherm and the relationship linking the standard free energy of adsorption to the equilibrium constant expressed in expression (13) [42], the values of ΔG^0_{ads} (kJ/mol) and K_{ads} were determined and presented in Table 5

$$\Delta G^0_{ads} = -RT\ln\left(55.5K_{ads}\right) \tag{13}$$

where, R is the ideal gas constant, T is the absolute temperature, and the value 55.5 is the concentration of water in the electrolyte in $mol \cdot L^{-1}$.

The behaviour of the curve shown in Figure 7 is linear with a slope near 1 and a correlation coefficient $R^2=1$. This suggests that the adsorption of the OER inhibitor at 298 K on the surface of the specimen in the 1 M HCl medium is performed using the Langmuir approach.

In accordance with the information cited in various papers, three modes of adsorption are possible. For $\Delta G^0_{ads} < -40\ kJ \cdot mol^{-1}$ the type of adsorption is chemical and for $\Delta G^0_{ads} > -20\ kJ \cdot mol^{-1}$ the adsorption is physical in nature, while for energies between $-40\ kJ \cdot mol^{-1}$ and $-20\ kJ \cdot mol^{-1}$ it is referred to as an adsorption of a mixed character [43]. About the OER product, the standard free energy of adsorption is $-45.73\ kJ \cdot mol^{-1}$. This value, which remains lower than $-40\ kJ \cdot mol^{-1}$, provides information about the chemical nature of the adsorption process of OER molecules. This process is the result of the

interactions between the vacant (*d*) orbitals of iron on the one hand and the free doublets of the oxygen atoms and unsaturated bonds of the inhibitor molecules on the other hand, thus leading to the formation of the covalent bonds between the OER molecules and the metal. The negative sign of ΔG^0_{ads} is attributed to the good stability of the formed protective layer of the adsorption mechanism [44]. The adhesion of the barrier formed at the metal/solution interface, which is due to the strong adsorption of OER compounds, is confirmed by the high values of the adsorption equilibrium constant K_{ads}.

Table 5. Thermodynamic parameters of OER adsorption on the steel surface in 1 M HCl at 298 K.

Inhibitor	K_{ads}, L/mol	R^2	ΔG_{ads}, kJ/mol
OER	$1.89 \cdot 10^6$	1	−45.73

3.4. Effect of temperature

Temperature is a factor influencing the characteristics of the metal and the inhibition phenomenon, while accelerating the dissolution rate of the film formed on the surface as the temperature rises [45]. In order to investigate the effect of this factor on the effectiveness of the OER inhibitor, electrochemical measurements were performed at temperatures ranging from 298 K to 328 K in the corrosive medium 1 M HCl in the absence and presence of the OER product with a concentration of 10^{-3} M, after 30 min immersion. The polarization curves are shown in Figures 8 and 9 and the electrochemical parameters are collected in Table 5.

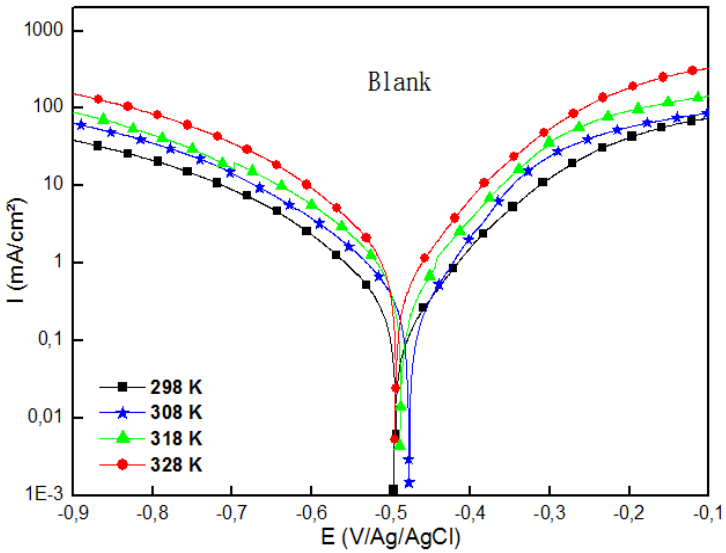

Figure 8. Potentiodynamic polarization curves of steel in 1 M HCl solution at different temperatures.

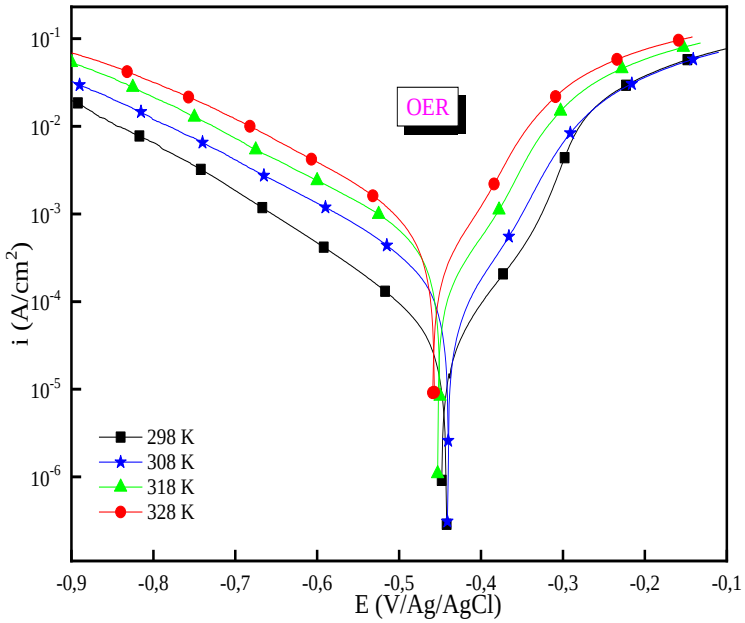

Figure 9. Polarization curves for steel in 1 M HCl solution in the presence of OER inhibitor with 10^{-3} M concentration at different temperatures.

Table 6. Electrochemical parameters for steel in 1 M HCl solution in the absence and presence of OER with 10^{-3} M concentration at different temperatures.

Medium	Temperature, K	E_{corr}, mV *vs.* Ag/AgCl	i_{corr}, μA·cm^{-2}	$-\beta_c$, mV·dec^{-1}	η_{PP}, %
Blank	298	−498	983	140	–
	308	−477	1200	184	–
	318	−487	1450	171	–
	328	−493	2200	161	–
OER	298	−442	46	166	95.3
	308	−440	115	159	90.4
	318	−448	206	157	85.8
	328	−456	334	148	84.8

The results presented in Table 6 clearly show that an increase in the densities of the corrosion currents, for the two inhibited and uninhibited solutions, is observed with the rise in temperature. Moreover, no change was observed in the shapes of the curves shown in Figures 8 and 9. From this, it can be deduced that the corrosion kinetics have undergone an acceleration, without any change in their electrochemical processes. Table 6 also shows that the increase in the corrosion rate with temperature was more marked in the virgin solution than in the inhibited solution, where this rise remains largely less important in the presence of OER molecules, with a slight decline in the efficiency. These results attest well the best

efficiency of steel corrosion inhibition by the OER product in the temperature range between 298 and 398 K [46].

3.5. Thermodynamic parameters of activation

The Arrhenius relation, given by expression (14), informs about the influence of temperature on the current density [47].

$$i_{corr} = Ke^{-\frac{E_a}{RT}} \tag{14}$$

with K, E_a, R, T and i_{corr} are successively the pre-exponential factor, the activation energy in $kJ \cdot mol^{-1}$, the perfect gas constant in $J \cdot mol^{-1} \cdot K^{-1}$, the absolute temperature in K and the corrosion current density in $mA \cdot cm^{-2}$.

Figure 10, which gives the evolution of $\ln(i_{corr})$ with the inverse of the absolute temperature for the blank and the inhibited solution, allowed for the evaluation of the activation energy.

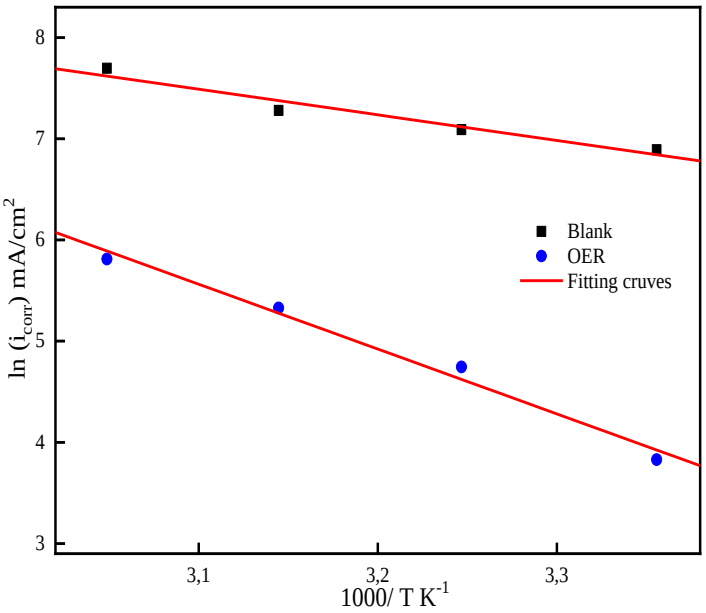

Figure 10. Arrhenius curve of steel in 1 M HCl medium without and in presence of OER at 10^{-3} M.

In order to evaluate the enthalpy ΔH_a and the entropy ΔS_a, formulas parallel to that of Arrhenius have been used, and they are given by Equations 15 and 16 [47].

$$i_{corr} = \frac{RT}{hN_a}\exp\left(\frac{\Delta S_a}{R}\right)\exp\left(\frac{\Delta H_a}{RT}\right) \tag{15}$$

$$\ln\left(\frac{i_{corr}}{T}\right) = \left[\ln\left(\frac{R}{hN_a}\right) + \frac{\Delta S_a}{R}\right] - \frac{\Delta H_a}{RT} \tag{16}$$

where h is Planck's constant, N_a is Avogadro's number, ΔH_a is the enthalpy of activation, and ΔS_a is the entropy of activation.

The variation of $\ln(i_{corr}/T)$ following the inverse of absolute temperature for the test and inhibited solutions is shown in Figure 11. The activation energies, enthalpies and entropies are grouped in Table 7.

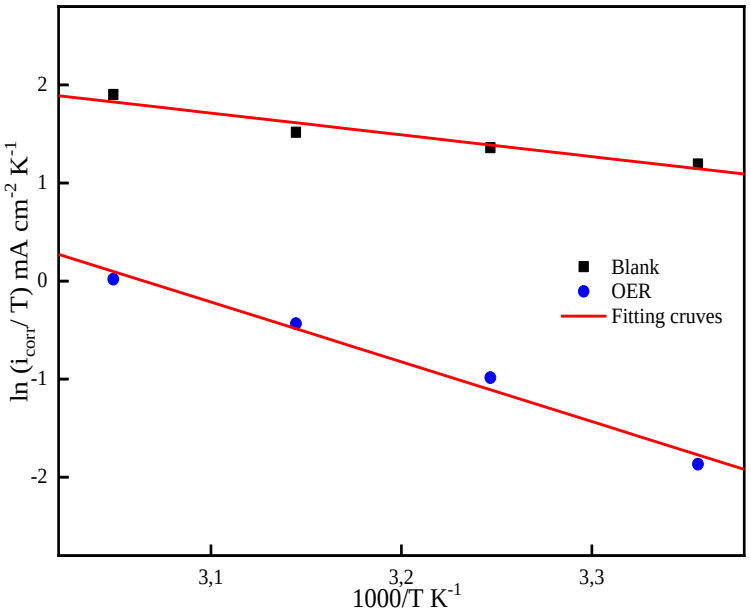

Figure 11. Variation of $\ln(i_{corr}/T)$ as a function of the inverse of the absolute temperature of steel in 1 M HCl without and in the presence of OER at 10^{-3} M.

Table 7. Activation parameters corresponding to the corrosion of steel in 1 M HCl without and with OER at the concentration of 10^{-3} M.

	E_a, kJ/mol	ΔH_a, kJ/mol	ΔS_a, J/mol·K
Blank	21.0	18.5	−126
OER	53.2	50.6	−42.5

Inspecting the values presented in Table 7, it is clear that the activation energy increased from 21.0 kJ·mol^{-1} to 53.2 kJ·mol^{-1} when the OER inhibitor was incorporated into the aggressive solution. This huge increase in activation energy can only be explained by an increase in the energy barrier of the corrosion reaction and the inhomogeneity of the film formed on the metal surface [48−51]. Moreover, ΔH_a for the inhibited solution is positive (endothermic process), which testifies that the adsorption of OER molecules on the steel surface is of the chemical type [52, 53]. Finally, the decrease of disorder accompanying the formation of the activated complex is attributed to the high value of entropy for the inhibited solution compared to that of the blank and to the negative signs of these entropies [54, 55].

3.6. Study of the metal surface by scanning electron microscopy (SEM) coupled to (EDS)

3.6.1. Scanning electron microscopy (SEM)

The morphological analysis of the steel surface was carried out with a scanning electron microscope (SEM), to complete the study of the film formed. This morphology concerning the steel sample after six hours of immersion in the 1 M HCl solution alone and with the OER inhibitor at a concentration of 10^{-3} M, at 298 K is given in Figure 12.

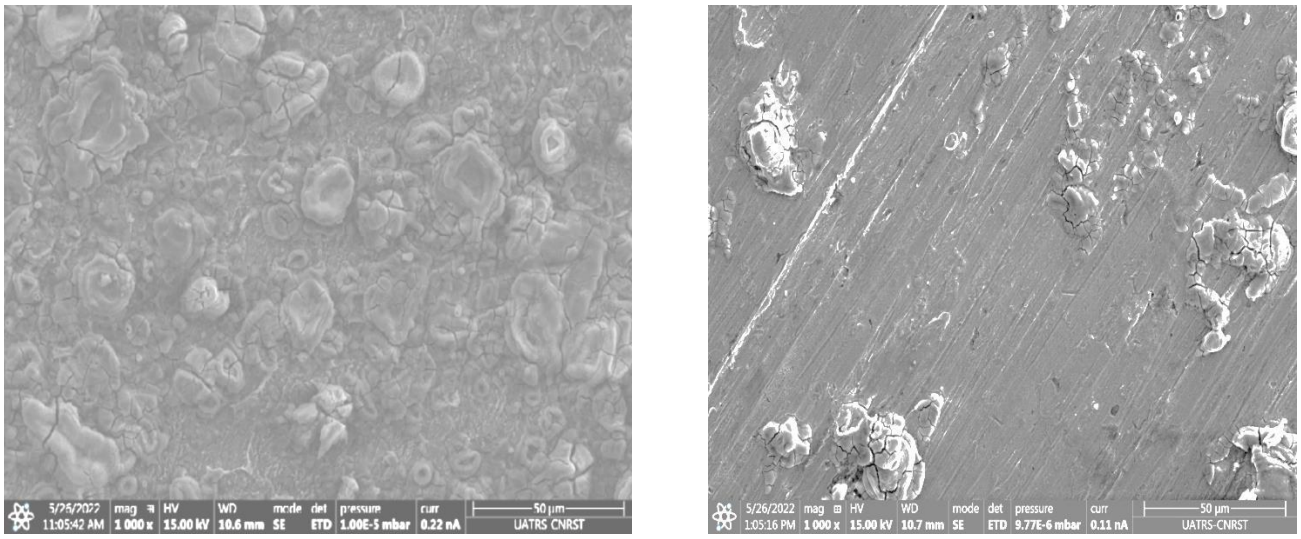

a b

Figure 12. MS surface morphology after 6 h immersion in 1 M HCl alone (a) and with 10^{-3} M of OER (b) at 298 K.

The image a of Figure 12 shows the emergence of the gray blocks evenly distributed over the entire surface of the metal, which explains the uniform dissolution of iron and formation of the iron oxides on the metal surface in the aggressive medium alone. After the addition of the OER inhibitor, image b in Figure 12, shows that the steel surface became smoother with the emergence of the crystallized platelets. This suggests the adsorption of the OER molecules on the surface by forming an adherent and stable film capable of protecting the steel by reducing the penetration of the electrolyte on its surface.

3.6.2. Energy dispersive X-Ray analysis (EDS)

The EDS spectrum in Figure 13a, shows the appearance of huge peaks corresponding to the elements oxygen and iron and weak peaks for carbon and chlorine, whose atomic proportions are shown in Table 8 (O=59.3%, Fe=36.9%, C=2.9%, Cl=1.0%). These results confirm the impact of the aggressive solution on the steel, which manifests itself by degradation, accelerated by the chloride ions, of its surface. This dissolution leads to the formation of iron oxides on the metal surface [56]. After the addition of the OER inhibitor, the EDS spectrum of Figure 13b shows an improvement in the percentage of iron accompanied by an appreciable drop in the oxygen ratio, which is due to the notable decrease in iron oxides on

the surface [57]. In addition, there is a relative increase in the carbon content and the extinction of the element chlorine, which are attributed to the deposition of organic compounds on the steel surface and the inability of the electrolyte to break through the metal-solution interface [57]. From all this, it can be affirmed that the adsorption of OER molecules on the surface of the substrate leads to the formation of a protective film that fights against the arrival of the products of the corrosive solution at this surface.

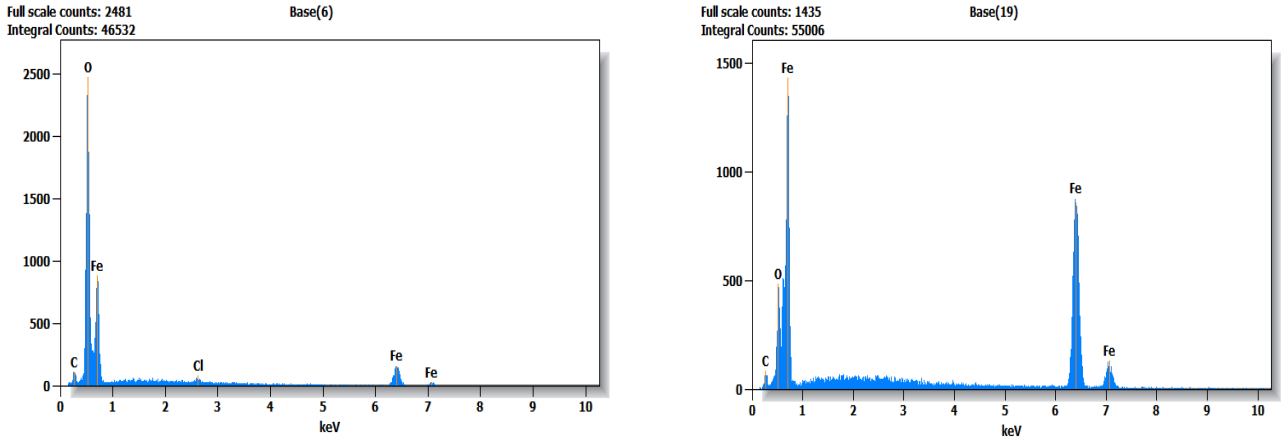

a b

Figure 13. Quantitative EDS of the surface condition after 6h of immersion of the steel in: 1 M HCl alone and with10^{-3} M of OER at 298 K.

Table 8. Atomic and mass percentages of the different elements resulting from the EDS analysis of the steel surface in 1 M HCl with and without OER inhibitor at 298 K.

	Element	Weight, %	Atom, %
EDS analysis of steel surface in 1.0 M HCl at 298 K	C	1.1	2.9
	O	30.8	59.3
	Cl	1.1	1.0
	Fe	67.0	36.9
	Total	100.0	100.0
EDS analysis of steel surface in 1.0 M HCl in the presence of OER at 298 K	C	1.2	4.9
	O	5.1	15.3
	Fe	93.6	79.8
	Total	100.0	100.0

3.7. Analysis of the reactivity descriptors

The structure minimization (most stable/lowest energy), electronic distributions of HOMO and LUMO are collected in Figure 14. The structure shown in this figure does not display

negative frequencies in the Gaussian 09 file, reflecting this well optimized representation. This result in a better delocalization of the HOMO and LUMO electron density at the level of this structure, consequently, the (HOMO/LUMO) distributions are almost situated on the same part of the OER epoxy resin. Such an electronic behaviour shows that the occupied part is well available for the reactivity and the donor attractor effect.

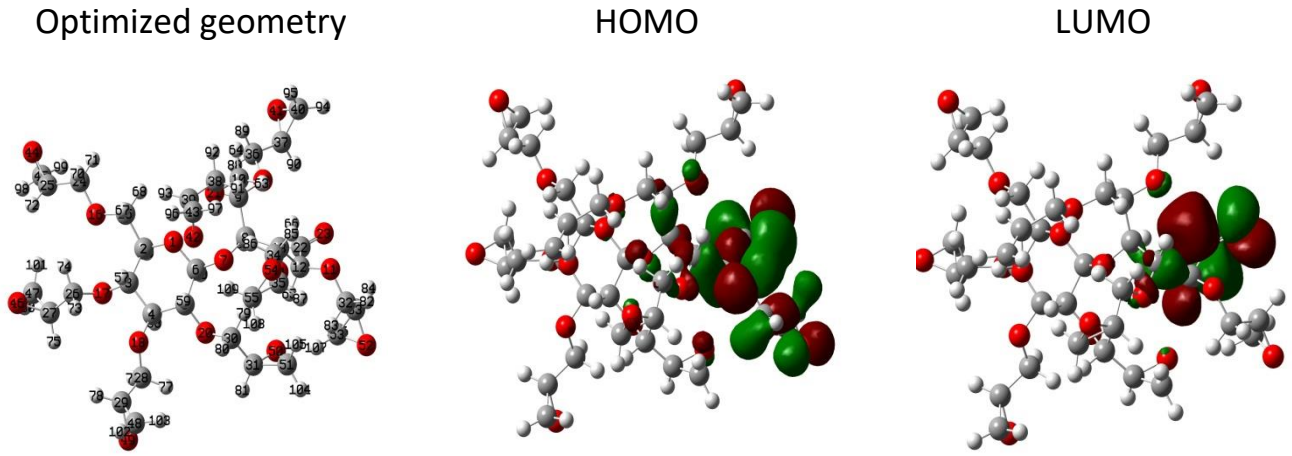

Figure 14. Optimized geometry with HOMO/LUMO localization density on OER.

The overall reactivity quantum descriptors are gathered in Table 8. It becomes clear from the quantum descriptor data of the neutral form that this last exhibits the smallest energy gap (ΔE_g=5.804 eV), giving the highest inhibitory effect [58]. This better chemical responsiveness is owed to the maximum value of E_{HOMO} (−6.756 eV) and the minimum value of E_{LUMO} (−0.952 eV). Electronegativity (χ) is another quantum descriptor that measures the ability of a chemical species to attract electrons. The high value of χ of iron (χ(Fe(110)=4.82 eV) in the surface than that of the inhibitor studied (3.854 eV) reflects an attractive effect of this element (Iron). The overall hardness (η) is used to measure the reactivity with respect to the electron donor capacity, where a higher value of the descriptor indicates a harder effect of an inhibitor molecule [59]. In the case investigated, the minimum value of η (2.902 eV) shows an inhibitory reactivity of OER with the iron surface. The number of electrons released from the optimized inhibitor to the vacant orbitals "*d*" of the iron d is quantified using ΔN_{110}, a high value of this descriptor denotes a large electron donor effect [60]. The value of 0.166 (ΔN_{110}) informs that OER able to easily donate electrons to form coordination bonds with the metal surface.

Table 9. Quantum chemical descriptors of OER molecule calculated using B3LYP/6-311++G(*d, p*) in aqueous phase.

Indices of OER	E_{HOMO}, **eV**	E_{LUMO}, **eV**	ΔE_g, **eV**	X, **eV**	H, **eV**	ΔN_{110}
	−6.756	−0.952	5.804	3.854	2.902	0.166

The local method based on the use of Fukui indices allows to determine the reactivity atoms that are responsible for the nucleophilic (f^+) and electrophilic (f^-) attacks. As a general rule, high values of both of these indices of the atoms in a molecular structure show a high donor effect for f^- and an attractor effect for f^+. This approach was carried out using the Dmol3 method with the GGA correlation exchange functional and the DNP base as reported in the work published by Benhiba *et al*. [61]. The calculation data are illustrated as curves in Figure 15. This figure displays only the atoms carrying a high density of Fukui functions used such that the atoms appeared are responsible on the local reactivity and result in more available coordination bonds enhancing the adsorption of the studied inhibitor on the metal support.

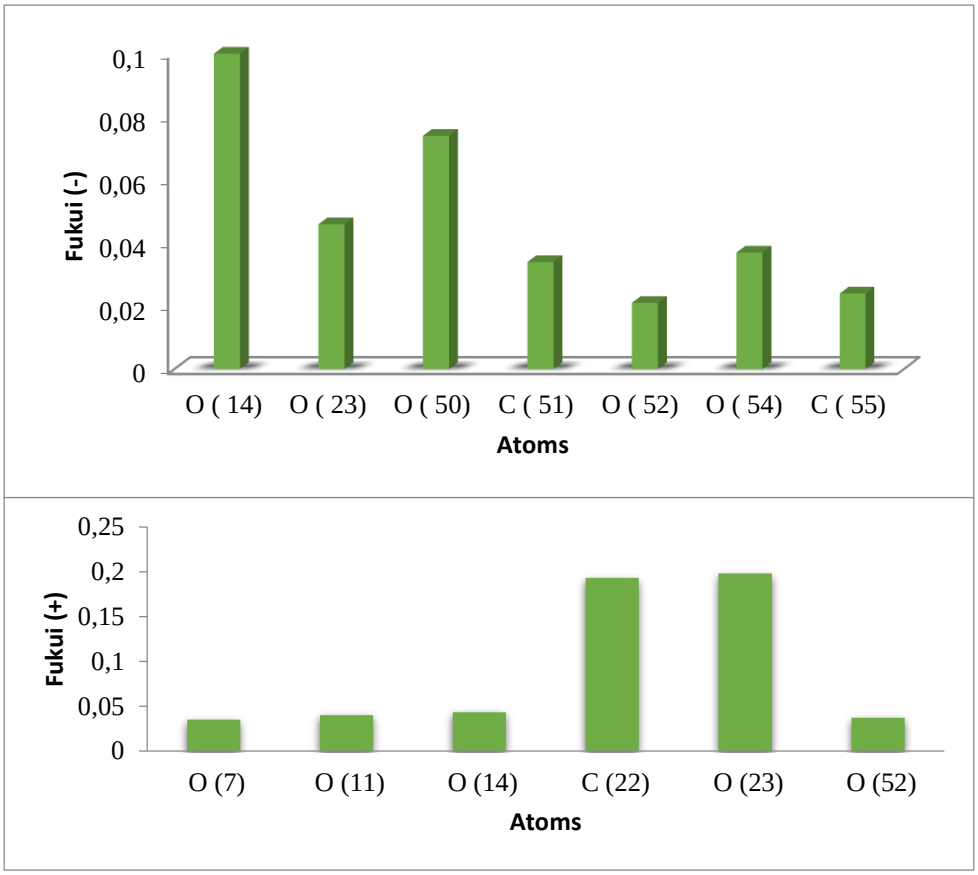

Figure 15. Fukui indices (f^+ and f^-) of the atoms for OER molecule.

3.8. MDS study

The aim of the present investigation is to evaluate and understand the way in which the neutral form operates on the iron atomic support. Furthermore, Figure 16 reproduces the best adsorption configuration OER on the chosen surface. As mentioned in these two views, the optimized pattern of the molecule takes up a substantial part of the Fe(110). Apparently, the fact that this adsorption property informs that there are several active acceptor/donor sites that contribute to the rise of the inhibition efficiency of the mentioned substance.

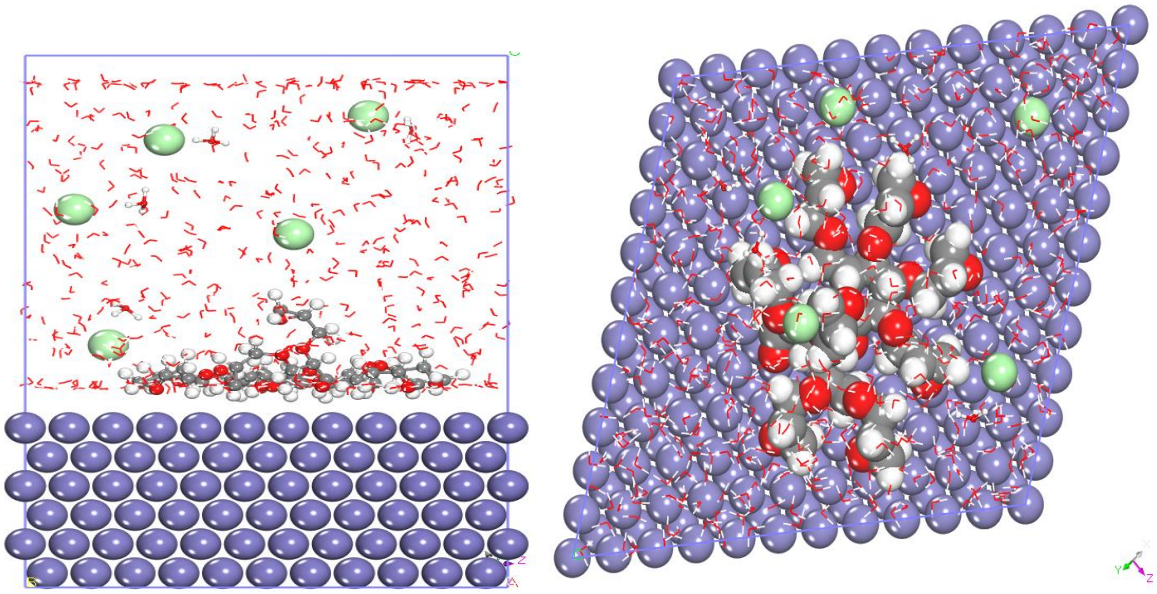

Figure 16. OER/Fe(110) system

The $E_{\text{interaction}}$ and E_{binding} values are defined by the two equations hereunder [62]:

$$E_{\text{interaction}} = E_{\text{total}} - (E_{\text{surface+solution}} + E_{\text{i}}) \quad (17)$$

$$E_{\text{binding}} = -E_{\text{interaction}} \quad (18)$$

The low value of $E_{\text{interaction}}$ attests to the interaction of OER with the interacting iron atoms, while the higher values of E_{binding} testify to a large adsorption [62].

The values of these two descriptors for the system are calculated, it appears from the comparative study that the most negative value of OER/Fe(110) (–984.754 kJ·mol^{-1}) reflects a larger interaction, while the highest value of E_{binding} (984.754 kJ·mol^{-1}) of this system indicates that the target molecule strongly binds to the investigated atomic layer.

3.9. RDF analysis

In order to better perceive the nature of the bonds occurring between the studied inhibitor and the Fe atoms, the radial distribution function (RDF) method is applied. The latter is a valuable tool for the determination of the Fe–OER interatomic distance [63]. The published literature confirmed that the likelihood of chemical adsorption was higher when the bond length was less than 3.5 Å. By contrast, physical adsorption is more probable [64]. In Figure 17, the spectral data from this method are illustrated. The first peak reveals that the bond lengths (OER–Fe) are less than 3.5 Å.

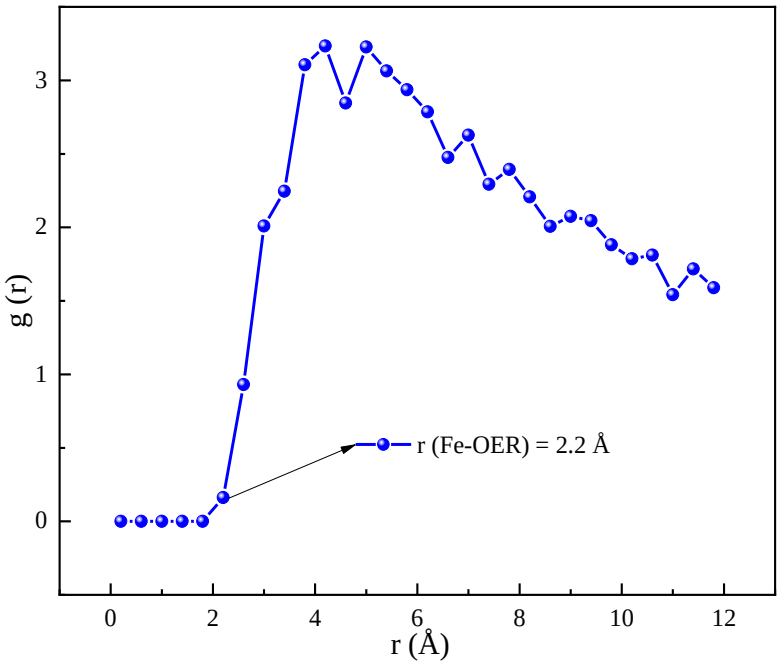

Figure 17. RDF of forms OER–Fe(110).

4. Conclusion

The synthetic compound ability to serve as a corrosion inhibition barrier makes it a more effective anticorrosive in HCl circumstances. According to the electrochemical investigation, the OER molecule adsorbed at the metal/electrolyte interface has an impact on both cathodic and anodic processes. The investigated new epoxy resin demonstrates how OER can create a shield above the metal plane to thwart corrosion by acting as a mixed-kind protector. Thermodynamic and activation factors limit the randomness of metal corrosion while highlighting the strong and endothermic inhibitory process. Also, the development of the inhibitor's protective barrier sitting on the metal surface, which reduces metal corrosion, is supported by morphological interpretations from SEM, and EDS. According to all of the findings and these morphological observations, the new epoxy resin facilitates effective adsorption with a maximal inhibition efficacy of 95.3%. Furthermore, DFT and MDS were implemented to check out the intersection among inhibition effectiveness and molecular structure, which were effectively complemented by the electrochemical experimental results.

References

1. M.A. Mazumder, Global Impact of Corrosion: Occurrence, Cost and Mitigation, *Global Journal of Engineering Sciences – GJES*, 2020, **5**, no. 4, 1–5. doi: 10.33552/GJES.2020.05.000618
2. R. Hsissou, H. Benassaoui, F. Benhiba, N. Hajjaji and A. Alharbi, Application of a new tri-functional epoxy prepolymer, triglycidyl ethylene ether of bisphenol a, in the coating of E24 steel in 3.5 % NaCl, *J. Chem. Technol. Metall.*, 2017, **52**, no. 3, 431–438.

3. R. Hsissou, S. Abbout, A. Berisha, M. Berradi, M. Assouag, N. Hajjaji and A. Elharfi, Experimental, DFT and molecular dynamics simulation on the inhibition performance of the DGDCBA epoxy polymer against the corrosion of the E24 carbon steel in 1.0M HCl solution, *J. Mol. Struct*., 2019, **1182**, 340–351. doi: 10.1016/j.molstruc.2018.12.030
4. A. Döner, R. Solmaz, M. Özcan and G. Kardaş, Experimental and theoretical studies of thiazoles as corrosion inhibitors for mild steel in sulphuric acid solution, *Corros. Sci*., 2011, **53**, no. 9, 2902–2913. doi: 10.1016/j.corsci.2011.05.027
5. C. Verma, V.S. Saji, M.A. Quraishi and E.E. Ebenso, Pyrazole Derivatives as environmental benign acid corrosion inhibitors for mild steel: Experimental and Computational Studies, *J. Mol. Liq*., 2020, **298**, 111943. doi: 10.1016/j.molliq.2019.111943
6. E.H. Norman, NACE Glossary of Corrosion Terms, *Mater. Prot*., 1965, **4**, no. 1, 79.
7. M. Faustina, A. Maciuk, P. Salvina, C. Roos and M. Lebrini, Corrosion inhibition of C38 steel by alkaloids extract of Geissospermum leave in 1M hydrochloric acid: Electrochemical and phytochemical studies, *Corros. Sci*., 2015, **92**, 287–300. doi: 10.1016/j.corsci.2014.12.005
8. M. Lebrini, F. Robert, A. Lecante and C. Roos, Corrosion inhibition of C38 steel in 1M hydrochloric acid medium by alkaloids extract from Oxandra asbeckii plant, *Corros. Sci*., 2011, **53**, no. 2, 687–695. doi: 10.1016/j.corsci.2010.10.006
9. M. Abouchane, N. Dkhireche, M. Rbaa, F. Benhiba, M. Ouakki, M. Galai, B. Lakhrissi, A. Zarrouk and M. Ebn Touhami, Insight into the corrosion inhibition performance of two quinoline-3-carboxylate derivatives as highly efficient inhibitors for mild steel in acidic medium: Experimental and theoretical evaluations, *J. Mol. Liq*., 2022, **360**, 119470. doi: 10.1016/j.molliq.2022.119470
10. P.A. Small, Some factors affecting the solubility of polymers, *J. Appl. Chem*., 1953, **3**, no. 2, 71–80. doi: 10.1002/jctb.5010030205
11. R. Hsissou, F. Benhiba, O. Dagdag, M. El Bouchti, K. Nouneh, M. Assouag, S. Briche, A. Zarrouk and A. Elharfi, Development and potential performance of prepolymer in corrosion inhibition for carbon steel in 1.0M HCl: Outlooks from experimental and computational investigations, *J. Colloid Interface Sci*., 2020, **574**, 43–60. doi: 10.1016/j.jcis.2020.04.022
12. R. Hsissou, S. Abbout, F. Benhiba, R. Seghiri, Z. Safi, S. Kaya, S. Briche, G. Serdaroğlu, H. Erramli, A. Elbachiri, A. Zarrouk and A. El Harfi, Insight into the corrosion inhibition of novel macromolecular epoxy resin as highly efficient inhibitor for carbon steel in acidic mediums: Synthesis, characterization, electrochemical techniques, AFM/UV–Visible and computational investigations, *J. Mol. Liq*., 2021, **337**, 116492. doi: 10.1016/j.molliq.2021.116492
13. R. Hsissou, F. Benhiba, S. About, O. Dagdag, S. Benkhaya, A. Berisha, H. Erramli and A. Elharfi, Trifunctional epoxy polymer as corrosion inhibition material for carbon steel in 1.0M HCl: MD simulations, DFT and complexation computations, *Inorg. Chem. Commun*., 2020, **115**, 107858. doi: 10.1016/j.inoche.2020.107858

14. R Hsissou, O. Dagdag, M. Berradi, M. El Bouchti, M. Assouag and A. Elharfi, Development rheological and anti-corrosion property of epoxy polymer and its composite, *Heliyon*, 2019, **5**, no. 11, E02789. doi: 10.1016/j.heliyon.2019.e02789
15. R. Hsissou, O. Dagdag, M. Berradi, M. El Bouchti, M. Assouag, A. El Bachiri and A. Elharfi, Investigation of structure and rheological behavior of a new epoxy polymer pentaglycidyl ether pentabisphenol A of phosphorus and of its composite with natural phosphate, *SN Appl. Sci*., 2019, **1**, 869. doi: 10.1007/s42452-019-0911-8
16. R. Hsissou, F. Benhiba, O. Dagdag, M. El Bouchti, K. Nouneh, M. Assouag, S. Briche, A. Zarrouk and A. Elharfi. Development and potential performance of prepolymer in corrosion inhibition for carbon steel in 1.0M HCl: Outlooks from experimental and computational investigations, *J. Colloid Interface Sci*., 2020, **574**, 43–60. doi: 10.1016/j.jcis.2020.04.022
17. H.M. Abd El-Lateef, M.A. Abo-Riya and A.H. Tantawy, Empirical and quantum chemical studies on the corrosion inhibition performance of some novel synthesized cationic Gemini surfactants on carbon steel pipelines in acid pickling processes, *Corros. Sci*., 2016, **108**, 94–110. doi: 10.1016/j.corsci.2016.03.004
18. T. Laabaissi, F. Benhiba, Z. Rouifi, M. Missioui, K. Ourrak, H. Oudda, Y. Ramli, I. Warad, M. Allali and A. Zarrouk, New quinoxaline derivative as a green corrosion inhibitor for mild steel in mild acidic medium: Electrochemical and theoretical studies, *Int. J. Corros. Scale Inhib*., 2019, **8**, no. 2, 241–256. doi: 10.17675/2305-6894-2019-8-2-6
19. M. Caricato, E. Frisch, J. Hiscocks and M.J. Frisch, *Gaussian 09: IOps Reference*, 2013, Wallingford, Gaussian, Inc., 170 pp.
20. M. Rbaa, M. Galai, F. Benhiba, I.B. Obot, H. Oudda, M. Ebn Touhami, B. Lakhrissi and A. Zarrouk, Synthesis and investigation of quinazoline derivatives based on 8-hydroxyquinoline as corrosion inhibitors for mild steel in acidic environment: experimental and theoretical studies, *Ionics*, 2018, **25**, 3473–3491.
21. H.C. Andersen, Molecular dynamics simulations at constant pressure and/or temperature, *J. Chem. Phys*., 1980, **72**, 2384–2393. doi: 10.1063/1.439486
22. Y. Kharbach, F.Z. Qachchachi, A. Haoudi, M. Tourabi, A. Zarrouk, C. Jama, L.O. Olasunkanmi, E.E. Ebenso and F. Bentiss, Anticorrosion performance of three newly synthesized isatin derivatives on carbon steel in hydrochloric acid pickling environment: Electrochemical, surface and theoretical studies, *J. Mol. Liq*., 2017, **246**, 302–316. doi: 10.1016/j.molliq.2017.09.057
23. J.O.M. Bockris and S. Srinivasan, Elucidation of the mechanism of electrolytic hydrogen evolution by the use of H-T separation factors, *Electrochim. Acta*, 1964, **9**, no. 1, 31–44. doi: 10.1016/0013-4686(64)80003-7
24. I. Nadi, Z. Belattmania, B. Sabour, A. Reani, A. Sahibed-dine, C. Jama and F. Bentiss, Sargassum muticum extract based on alginate biopolymer as a new efficient biological corrosion inhibitor for carbon steel in hydrochloric acid pickling environment:

Gravimetric, electrochemical and surface studies, *Int. J. Biol. Macromol*., 2019, **141**, 137–149. doi: 10.1016/j.ijbiomac.2019.08.253
25. M.S. Al-Otaibi, A.M. Al-Mayouf, M. Khan, A.A. Mousa, S.A. Al-Mazroa and H.Z. Alkhathlan, Corrosion inhibitory action of some plant extracts on the corrosion of mild steel in acidic media, *Arabian J. Chem*., 2014, **7**, no. 3, 340–346. doi: 10.1016/j.arabjc.2012.01.015
26. I. Ahamad and M.A. Quraishi, Mebendazole: New and efficient corrosion inhibitor for mild steel in acid medium, *Corros. Sci*., 2010, **52**, no. 2 651–656. doi: 10.1016/j.corsci.2009.10.012
27. J.O. Bockris, Electrons, Interfaces, and Societies in the 21st Century, *Electrochem. Transition*, 1992, 227–322. doi: 10.1007/978-1-4615-9576-2_17
28. M.A. Hegazy, A.M. Badawi, S.S. Abd El Rehim and W.M. Kamel, Corrosion inhibition of carbon steel using novel N-(2-(2-mercaptoacetoxy)ethyl)-N,N-dimethyl dodecan-1-aminium bromide during acid pickling, *Corros. Sci*., 2013, **69**, 110–122. doi: 10.1016/j.corsci.2012.11.031
29. S. Ramesh and S. Rajeswari, Corrosion inhibition of mild steel in neutral aqueous solution by new triazole derivatives, *Electrochim. Acta*, 2004, **49**, no. 5, 811–820. doi: 10.1016/j.electacta.2003.09.035
30. D.K. Singh, S. Kumar, G. Udayabhanu and R.P. Johnn, 4(N,N-dimethylamino) benzaldehy- deni- cotinichydrazone as corrosion inhibitor for mild steel in 1M HCl solution: an experimental and theoretical study, *J. Mol. Liq*., 2016, **216**, 738–746. doi: 10.1016/j.molliq.2016.02.012
31. Y. El aoufir, S. Zehra, H. Lgaz, A. Chaouiki, H. Serrar, S. Kaya, R. Salghi, S.K. AbdelRaheem, S. Boukhris, A. Guenbour and I.-M. Chung, Evaluation of inhibitive and adsorption behavior of thiazole-4-carboxylates on mild steel corrosion in HCl, *Colloids Surf., A*, 2020, **606**, 125351. doi: 10.1016/j.colsurfa.2020.125351
32. A.O. Yüce and G. Kardaş, Adsorption and inhibition effect of 2-thiohydantoin on mild steel corrosion in 0.1M HCl, *Corros. Sci*., 2012, **58**, 86–94. doi: 10.1016/j.corsci.2012.01.013
33. H. Ashassi-Sorkhabi, B. Shaabani and D. Seifzadeh, Corrosion inhibition of mild steel by some schiff base compounds in hydrochloric acid, *Appl. Surf. Sci*., 2005, **239**, no. 2, 154–164. doi: 10.1016/j.apsusc.2004.05.143
34. K. Hu, J. Zhuang, C. Zheng, Z. Ma, L. Yan, H. Gu, X. Zeng and J. Ding, Effect of novel cytosine-L-alanine derivative-based corrosion inhibitor on steel surface in acidic solution, *J. Mol. Liq*., 2016, **222**, 109–117. doi: 10.1016/j.molliq.2016.07.008
35. B. Ramezanzadeh, S.Y. Arman, M. Mehdipour and B.P. Markhali, Analysis of electrochemical noise (ECN) data in time and frequency domain for comparison corrosion inhibition of some azole compounds on Cu in 1.0M H_2SO_4 solution, *Appl. Surf. Sci*., 2014, **289**, 129–140. doi: 10.1016/j.apsusc.2013.10.119

36. M. Bouanis, M. Tourabi, A. Nyassi, A. Zarrouk, C. Jama and F. Bentiss, Corrosion inhibition performance of 2,5-bis(4-dimethylaminophenyl)-1,3,4-oxadiazole for carbon steel in HCl solution: Gravimetric, electrochemical and XPS studies, *Appl. Surf. Sci*., 2016, **389**, 952–966. doi: 10.1016/j.apsusc.2016.07.115
37. M.P. Chakravarthy and K.N. Mohana, Adsorption and corrosion inhibition characteristics of some nicotinamide derivatives on mild steel in hydrochloric acid solution, *Int. Scholarly Res. Not*., 2014, **2014**, 1–13. doi: 10.1155/2014/687276
38. I.B. Obot and I.B. Onyeachu, Electrochemical frequency modulation (EFM) technique: Theory and recent practical applications in corrosion research, *J. Mol. Liq*., 2018, **249**, 83–96. doi: 10.1016/j.molliq.2017.11.006
39. I. Danaee and P. Nikparsa, Electrochemical Frequency Modulation, Electrochemical Noise, and Atomic Force Microscopy Studies on Corrosion Inhibition Behavior of Benzothiazolone for Steel API X100 in 10% HCl Solution, *J. Mater. Eng. Perform*., 2019, **28**, 5088–5103. doi: 10.1007/s11665-019-04272-z
40. R.W. Bosch, J. Hubrecht, W.F. Bogaerts and B.C. Syrett, Electrochemical frequency modulation: A new electrochemical technique for online corrosion monitoring, *Corrosion*, 2001, **57**, no. 1, 60–70. doi: 10.5006/1.3290331
41. M. Faustin, A. Maciuk, P. Salvin, C. Roos and M. Lebrini, Corrosion inhibition of C38 steel by alkaloids extract of *Geissospermum laeve* in 1M hydrochloric acid: Electrochemical and phytochemical studies, *Corros. Sci*., 2015, **92**, 287–300. doi: 10.1016/j.corsci.2014.12.005
42. C. Verma, V.S. Saji, M.A. Quraishi and E.E. Ebenso, Pyrazole derivatives as environmental benign acid corrosion inhibitors for mild steel: Experimental and computational studies, *J. Mol. Liq*., 2020, **298**, 111943. doi: 10.1016/j.molliq.2019.111943
43. M. Abouchane, N. Dkhireche, M. Rbaa, F. Benhiba, M. Ouakki, M. Galai, B. Lakhrissi, A. Zarrouk and M. Ebn Touhami, Insight into the corrosion inhibition performance of two quinoline-3-carboxylate derivatives as highly efficient inhibitors for mild steel in acidic medium: Experimental and theoretical evaluations, *J. Mol. Liq*., 2022, **360**, 119470. doi: 10.1016/j.molliq.2022.119470
44. Y. El aoufir, S. Zehra, H. Lgaz, A. Chaouiki, H. Serrar, S. Kaya, R. Salghi, S.K. AbdelRaheem, S. Boukhris, A. Guenbour and I.-M. Chung, Evaluation of inhibitive and adsorption behavior of thiazole-4-carboxylates on mild steel corrosion in HCl, *Colloids Surf., A*, 2020, **606**, 125351. doi: 10.1016/j.colsurfa.2020.125351
45. N. Gharda, M. Galai, L. Saqalli, N. Habbadi, R. Ghailane, A. Souizi, M. Ebn Touhami and Y. Peres-Lucchese, Linseed oil as a novel eco-friendly corrosion inhibitor of carbon steel in 1M HCl, *Surf. Rev. Lett*., 2019, **26**, no. 2, 1850148. doi: 10.1142/S0218625X18501482
46. I.B. Obot and N.O. Obi-Egbedi, Theoretical study of benzimidazole and its derivatives and their potential activity as corrosion inhibitors, *Corros. Sci*., 2010, **52**, no. 2, 657–660. doi: 10.1016/j.corsci.2009.10.017

47. N. Errahmany, M. Rbaa, A.S. Abousalem, A. Tazouti, M. Galai, E.H.El Kafssaoui, M. Ebn Touhami, B. Lakhrissi and R. Touir, Experimental, DFT calculations and MC simulations concept of novel quinazolinone derivatives as corrosion inhibitor for mild steel in 1.0M HCl medium, *J. Mol. Liq*., 2020, **312**, 113413. doi: 10.1016/j.molliq.2020.113413
48. S.M. Shaban, A.A. Abd-Elaal and S.M. Tawfik, Gravimetric and electrochemical evaluation of three nonionic dithiol surfactants as corrosion inhibitors for mild steel in 1M HCl solution, *J. Mol. Liq*., 2016, **216**, 392–400. doi: 10.1016/j.molliq.2016.01.048
49. M. Rbaa, M. Galai, Y. El Kacimi, M. Ouakki, R. Touir, B. Lakhrissi and M. Ebn Touhami, Adsorption properties and inhibition of carbon steel corrosion in a hydrochloric solution by 2-(4,5-diphenyl-4,5-dihydro-1H-imidazol-2-yl)-5-methoxyphenol, *Port. Electrochim. Acta*, 2017, **35**, no. 6, 323–338. doi: 10.4152/pea.201706323
50. G.K. Gomma and M.H. Wahdan, Schiff bases as corrosion inhibitors for aluminium in hydrochloric acid solution, *Mater. Chem. Phys*., 1995, **39**, no. 3, 209–213. doi: 10.1016/0254-0584(94)01436-K
51. S.A. Ali, A. El-Shareef, R. Al-Ghamdi and M.T. Saeed, The isoxazolidines: the effects of steric factor and hydrophobic chain length on the corrosion inhibition of mild steel in acidic medium, *Corros. Sci*., 2005, **47**, no. 11, 2659–2678. doi: 10.1016/j.corsci.2004.11.007
52. F. Bentiss, M. Lebrini and M. Lagrenee, Thermodynamic characterization of metal dissolution and inhibitor adsorption processes in mild steel/2,5-bis(n-thienyl)-1,3,4-thiadiazoles/hydrochloric acid system, *Corros. Sci*., 2005, **47**, no. 12, 2915–2931. doi: 10.1016/j.corsci.2005.05.034
53. G.N. Mu, X. Li and F. Li, Synergistic inhibition between o-phenanthroline and chloride ion on cold rolled steel corrosion in phosphoric acid, *Mater. Chem. Phys*., 2004, **86**, no. 1, 59–68. doi: 10.1016/j.matchemphys.2004.01.041
54. S. Martinez and I. Stern, Thermodynamic characterization of metal dissolution and inhibitor adsorption processes in the low carbon steel/mimosa tannin/sulfuric acid system, *Appl. Surf. Sci*., 2002, **199**, no. 1–4, 83–89. doi: 10.1016/S0169-4332(02)00546-9
55. M. Yadav, S. Kumar, N. Tiwari, I. Bahadur and E.E. Ebenso, Experimental and quantum chemical studies of synthesized triazine derivatives as an efficient corrosion inhibitor for N80 steel in acidic medium, *J. Mol. Liq*., 2015, **212**, 151–67. doi: 10.1016/j.molliq.2015.09.019
56. F. El Hajjaji, F. Abrigach, O. Hamed, A.R. Hasan, M. Taleb, S. Jodeh, E. Rodriguez-Castellón, M.V.M. de Yuso and M. Algarra, Corrosion resistance of mild steel coated with orgainc material containing pyrazolmoiety, *Coatings*, 2018, **8**, no. 10, 330. doi: 10.3390/coatings8100330

57. F. Bentiss, M. Lebrini and M. Lagrenee, Thermodynamic characterization of metal dissolution and inhibitor adsorption processes in mild steel/2,5-bis(*n*-thienyl)-1,3,4-thiadiazoles/hydrochloric acid system, *Corros. Sci*., 2005, **47**, no. 12, 2915–2931. doi: 10.1016/j.corsci.2005.05.034
58. U.P. Kumar, R.H. Albrakaty, N. Wazzan, I.B. Obot, Z.S. Safi, S. Shanmugan and T. Liang, Insight into the nature of the ionic interactions between some aldehydes and Ni-W alloy: A theoretical study, *Mater. Today Commun*., 2020, **22**, 100693. doi: 10.1016/j.mtcomm.2019.100693
59. M. El Faydy, F. Benhiba, H. About, Y. Kerroum, A. Guenbour, B. Lakhrissi, I. Warad, C. Verma, El-S. M. Sherif, E.E. Ebenso and A. Zarrouk, Experimental and computational investigations on the anti-corrosive and adsorption behavior of 7-*N*,*N*′-dialkyaminomethyl-8-Hydroxyquinolines on C40E steel surface in acidic medium, *J. Colloid Interface Sci*., 2020, **576**, 330–344. doi: 10.1016/j.jcis.2020.05.010
60. Y. Kharbach, F.Z. Qachchachi, A. Haoudi, M. Tourabi, A. Zarrouk, C. Jama, L.O. Olasunkanmi, E.E. Ebenso and F. Bentiss, Anticorrosion performance of three newly synthesized isatin derivatives on carbon steel in hydrochloric acid pickling environment: Electrochemical, surface and theoretical studies, *J. Mol. Liq*., 2017, **246**, 302–316. doi: 10.1016/j.molliq.2017.09.057
61. F. Benhiba, R. Hsissou, K. Abderrahim, H. Serrar, Z. Rouifi, S. Boukhris, G. Kaichouh, A. Bellaouchou, A. Guenbour, H. Oudda, I. Warad and A. Zarrouk, Development of New Pyrimidine Derivative Inhibitor for Mild Steel Corrosion in Acid Medium, *J. Bio Tribo Corros*., 2022, **8**, no. 36. doi: 10.1007/s40735-022-00637-5
62. F. Benhiba, N.K. Sebbar, H. Bourazmi, M.E. Belghiti, R. Hsissou, T. Hökelek, A. Bellaouchou, A. Guenbour, I. Warad, H. Oudda, A. Zarrouk and E.M. Essassi, Corrosion inhibition performance of 4-(prop-2-ynyl)-[1,4]-benzothiazin-3-one against mild steel in 1M HCl solution: Experimental and theoretical studies, *Int. J. Hydrogen Energy*, 2021, **46**, no. 51, 25800–25818. doi: 10.1016/j.ijhydene.2021.05.091
63. V. Mehmeti and F.I. Podvorica, Experimental and Theoretical Studies on Corrosion Inhibition of Niobium and Tantalum Surfaces by Carboxylated Graphene Oxide, *Materials*, 2018, **11**, no. 6, 893. doi: 10.3390/ma11060893
64. S.G. Charati and S.A. Stern, Diffusion of Gases in Silicone Polymers: Molecular Dynamics Simulations, *Macromolecules*, 1998, **31**, no. 16, 5529–5535. doi: 10.1021/ma980387e

♦ ♦ ♦